Reduction of material mass of optical component in cryogenic camera by using high-order Fresnel lens on a thin germanium substrate

Tatiana Grulois, Guillaume Druart, Hervé Sauer, Mathieu Chambon, Nicolas Guérineau, Serge Magli, Gillles Lasfargues, Pierre Chavel

Reduction of material mass of optical component in cryogenic camera by using high-order Fresnel lens on a thin germanium substrate

Tatiana Grulois,[1,*] Guillaume Druart,[1] Hervé Sauer,[2] Mathieu Chambon,[1] Nicolas Guérineau,[1] Serge Magli,[3] Gillles Lasfargues,[4] and Pierre Chavel[2]

[1]ONERA, Chemin de la Hunière, 91123 Palaiseau Cedex, France
[2]Laboratoire Charles Fabry, Institut d'Optique, CNRS, 2 Avenue Augustin Fresnel, 91127 Palaiseau Cedex, France
[3]SOFRADIR, ZI-BP21, 38113 Veurey-Voroize, France
[4]CEA LETI Minatec, 17 rue des Martyrs, 38054 Grenoble Cedex, France
*Corresponding author: tatiana.grulois@onera.fr

We designed a compact infrared cryogenic camera using only one lens mounted inside the detector area. In the field of cooled infrared imaging systems, the maximal detector area is determined by the dewar. It is generally a sealed and cooled environment dedicated to the infrared quantum detector. By integrating an optical function inside it, we improve the compactness of the camera as well as its performances. The originality of our approach is to use a thin integrated optics which is a high quality Fresnel lens on a thin germanium substrate. The aim is to reduce the additional mass of the optical part integrated inside the dewar to obtain almost the same cool down time as a conventional dewar with no imaging function. A prototype has been made and its characterization has been carried out.

1. INTRODUCTION

Today, significant efforts are made to develop miniaturized infrared cameras in order to provide small payload systems with thermal vision capability for both military and civilian applications. Reducing the size and the weight of infrared cameras then leads to reduced fabrication costs and offers the opportunity to open new markets.

In the cooled infrared domain, imaging systems consist of optical elements followed by a quantum detector. The detector is contained in a vacuum-sealed cryogenically cooled environment called a detector-dewar-cooled-assembly (DDCA) and lenses are traditionally located outside the detector area. In recent years, it has been shown that it is possible to design compact cooled infrared cameras by breaking down the technological barriers of limited DDCA volume and by integrating optics directly inside the dewar [1–4]. Indeed, a cold shield is located inside traditional dewar assemblies and can be used as a mechanical mount for optical components.

In the literature, some optical design completely integrated inside the DDCA have recently been suggested. In [1], a prototype compatible with wide field applications is presented but due to its small F-number, its architecture is quite complex. Thus, the system is made of one warm dome lens replacing the window and three cold refractive lenses. In [2] another cooled infrared system with optics integrated inside the dewar is presented, but the design also potentially involves several cold optical elements.

Although the compactness is improved, the drawback of these imagers is that they involve a relatively significant additional optical mass inside the DDCA. If the cooled mass is increased, the cool down time will be increased accordingly. Moreover, it is worth mentioning that adding optical elements inside the cold shield tends to change the trade-off in the mechanical design of the cold shield as well, and thus it tends to increase the mass of the cold shield too. A codesign between optical design and cold shield architecture helps reducing the overall mass to be cooled [3].

For several years, our team has been working on infrared optical designs that are more compatible with the cryogenic environment of the dewar. Indeed, some trade-off on the F-number have been considered and efforts have been made in limiting the additional mass of the integrated optics. Thus, a first imager called SOIE camera has been developed in [4] by integrating a very simple meniscus inside the cold shield.

However, since the design is based on a landscape lens architecture, the overall length of this system is twice the focal length of the camera. For that reason, the focal length must be small if we want to limit the size of the optical mount to the size of conventional cold shields.

Thus, some subsequent works have consisted in reducing further the total length of the optical design by exploring multichannel architectures. The aim was to integrate optical components directly on the IR detector. As discussed in [5], decreasing the focal length of the system while maintaining a constant FOV and a constant f-number results in a decrease of the angular resolution and of the number of resolved points. However, a solution to overcome this problem is to design a multichannel system based on the TOMBO principle [6]. It consists in splitting the sampling of the scene into different channels. Thus, in [7] our team suggested a very thin cryogenic multichannel wafer-level infrared camera directly integrated on the infrared focal plane array. It is based on TOMBO principle and it consists of two microlens arrays. The total length of the suggested system is less than 5 mm.

In this paper another design strategy for reducing the integrated optical mass is suggested. We propose a compact cooled infrared camera with almost the same cool down time as a conventional camera with optics located outside the dewar. Our work is based on a *minimalist approach* detailed in Section 2. It consists in providing an imaging property to the DDCA without any additional mass, by providing an imaging function to thin optical plates that are found in conventional dewars. The design of our camera is described in Section 3. It is based on a landscape lens architecture made of a cold diaphragm, a cold high-order Fresnel lens on a thin germanium plate, and the cooled detector. Section 4 presents the experimental characterization of our camera and shows some images obtained with our prototype. Results are then compared to the experimental performances of the SOIE camera.

2. STRATEGY TO DESIGN A COMPACT CRYOGENIC CAMERA WITH LIMITED COOL DOWN TIME

A. Description of the Detector Area

Our field of research is about the design of a compact cooled infrared camera operating in the mid-wavelength infrared (MWIR) spectral range, from around 3–5 μm. At these wavelengths, most of detectors are based on quantum detectors technology and for maximum sensitivity they need to be cryogenically cooled to liquid nitrogen temperature (77 K). For that purpose they are mounted inside a dewar detector cooled assembly (DDCA).

A typical DDCA is illustrated in Fig. 1. It is a hermetic vaccum-sealed environment where the detector is cooled on a cold plate. A window opens the dewar while maintaining its airtightness. Moreover, within the DDCA is a cold shield made of one cold diaphragm and one cold filter. The cold diaphragm limits the angle over which the detector sees the scene to reduce the background current and the cold filter restrains the spectral bandwidth of the detector.

B. Minimalist Approach

For designing a compact imager in the cooled infrared domain, some recent works have consisted in integrating the optics directly inside the dewar but they tend to increase the cool down time. To improve the compactness of cooled infrared cameras without increasing the time of the cooling process, we propose here an innovative strategy based on a *minimalist approach*. It consists in giving an imaging property to the dewar without integrating any additional mass inside the DDCA. As mentioned in the previous subsection, commercially available dewars already contain several optical components: a window, a cold diaphragm, and a cold filter. These optical elements are thin plates with no optical power. By giving an imaging function to one of these thin optical plates, we will design a very compact imager with the same cool down time as a conventional bulky camera without integrated optics.

In previous work [8], a compact infrared design based on a *minimalist approach* has been proposed already. As a first step in the miniaturization, the cold diaphragm of the DDCA was replaced by a pinhole that behaves as the only focusing element. This way the DDCA became a real *camera obscura*. Then, the window has been replaced by a fisheye lens in order to widen the angular acceptance of the design. Despite advantages in terms of depth of field and field of view, this design suffers from low gathering efficiency and low resolution. In order to achieve better optical performances, we aim at giving an imaging function to the cold filter by replacing it by a thin optics.

3. OPTICAL DESIGN

A. Evolution of the SOIE Camera

Our approach consists in proposing an evolution of the cooled infrared camera called SOIE [4]. This is a prototype mentioned

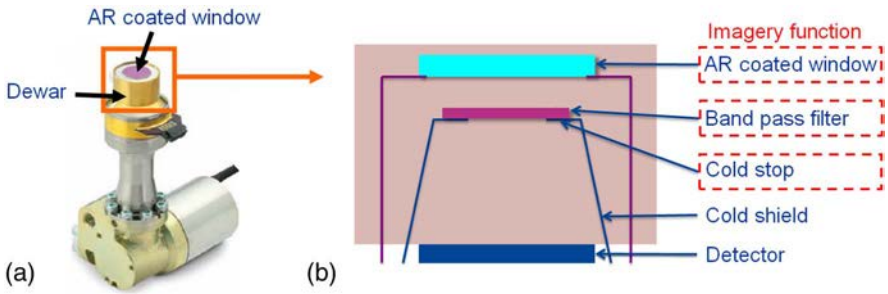

Fig. 1. Illustration of our minimalist approach: giving an imaging function to the DDCA without any additional mass. (a) External view of a DDCA commercialized by the French company Sofradir. (b) Illustration of a cold shield.

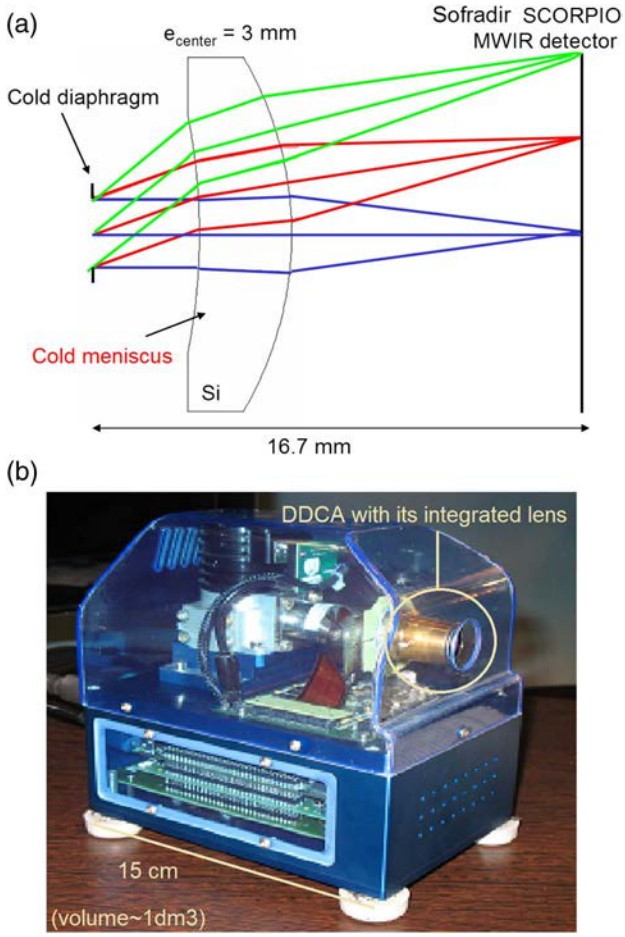

Fig. 2. (a) Setup of the landscape lens SOIE camera made of one cold meniscus in silicon integrated inside the DDCA. (b) Illustration of the SOIE demonstrator [3].

in the introduction, with one integrated optical element inside the cold shield. In Fig. 2(a) is shown the optical architecture and in Fig. 2(b) the demonstrator is illustrated. The integrated optics is a relatively thick meniscus in silicon that has a center thickness of 3 mm. The sag heights of this component are 0.39 mm on the left side and 1.63 mm on the right side, and the overall mass of the meniscus is equal to 0.73 g. Our strategy consists in designing an imager that has the same first order optical characteristics as the SOIE camera but that integrates a thinner and lighter optics in order to decrease the time of the cooling process. For that purpose, a nearly flat diffractive lens will be used and would directly replace the cold filter of the DDCA.

B. Toward an Optical System Design with Integrated High-Order Fresnel Lens

In recent years, diffractive optical elements have generated great interest in many fields of applications over the entire spectral range, some of them we can mention here. In the visible spectral range diffractive lenses have been recently used for their advantages in terms of weight, size and cost when designing large rear projection devices [9] or achromatic high-concentration photovoltaic systems [10,11]. They have also been suggested for imaging with extended depth of field for visible medical applications [12]. Moreover, a system design for operation in the ultraviolet spectral range that uses two light and low-absorbing Fresnel lenses for cosmic ray observation has been suggested in [13]. In the infrared spectral range, diffractive microlenses have been proposed for example for improving the performances of focal plane arrays [14]. As a final example, diffractive optics have also shown recent interest for broadband applications in the THz range [15].

In this paper, we aim at designing a single thin diffractive lens system for broadband and wide field of view imaging applications in the infrared domain. As we recently mentioned in [16], a high-order Fresnel lens can be a good candidate when designing a broadband microimager in IR spectrum. Indeed, while traditional low-order Fresnel lenses exhibit strong chromaticity making them unproper for broadband imagery, working in a higher diffraction order can significantly reduce chromatic aberrations as shown in the 90's [17–20]. In [16], the uncooled camera we suggested is based on a small microbolometer array. It operates in the long-wavelength infrared (LWIR) spectral range and is dedicated to low-cost surveillance applications. For that reason, a thin Fresnel lens in silicon is used and the chosen etching depth corresponds to state of art etching depth achievable when manufacturing a Fresnel lens by photolithography.

In the current study, we aim at designing a cooled MWIR camera. Dedicated markets are high-performance and high-sensitivity applications. Design constraints are thus limited by optical performances rather than final fabrication cost. In particular, the Fresnel lens can be made in germanium rather than silicon. Due to its high refractive index, low dispersion and low absorption, it is the material of choice for the design of quality infrared imaging systems. Germanium also offers a manufacturing advantage when generating an effective continuous Fresnel profile with large etching depth by diamond turning process [21]. Indeed, germanium is easier to machine than silicon because of lower tool wear rate [22–24]. Due to recent developments in the diamond turning process and thanks to sharp cutting edges of diamond tools, a germanium Fresnel lens with large etching depth can currently be made by direct diamond turning with very high efficiency [25,26].

Thanks to higher index of refraction, lower nominal wavelength and higher etching depth than developed in [16], a very high nominal diffraction order of the Fresnel lens is easily achievable. Within given conditions, the higher the nominal diffraction order, the smaller are induced chromatic aberrations. Moreover, working in the MWIR spectral range rather than in the LWIR spectral range also tends to limit diffractive chromatism. Chromatic aberrations of our Fresnel lens will be detailed below.

C. Description of Selected Optical Design

The selected optical design is illustrated in Fig. 3. It consists of a landscape lens architecture with same optical parameters as SOIE camera: it has a field of view of ±30° on the length of a Sofradir SCORPIO detector made of 640 × 512 pixels with 15 μm pixel pitch, it has a F-number of 4 and an effective focal length of 9.6 mm.

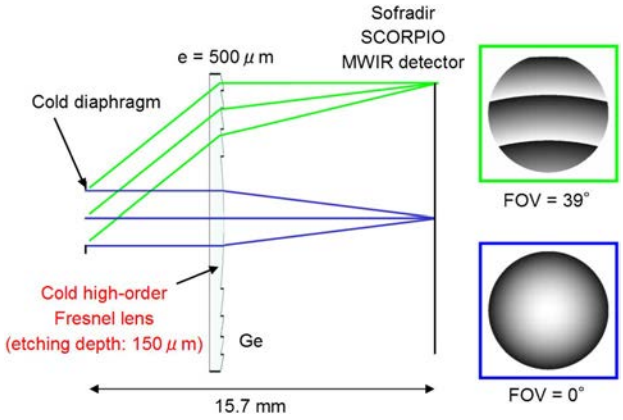

Fig. 3. Setup of the MWIR landscape lens as implemented with a high order Fresnel lens in germanium integrated inside the DDCA. The etching depth is equal to 150 μm.

The relatively thick meniscus used in SOIE camera has been replaced by a high-order Fresnel lens etched on the detector-side surface of a 500 μm-thick plate made of germanium. The etching depth of the Fresnel profile is equal to 150 μm.

The replacement of the meniscus lens of the SOIE camera by a 500 μm-thick Fresnel lens leads to a significant reduction of the integrated material mass. Indeed, while the mass of the SOIE silicon meniscus itself, ignoring opto-mechanical constraints, is 0.45 g, it is only 0.25 g for the germanium Fresnel lens of our camera. Because of opto mechanical requirements, the component diameter needs to be slightly larger than the clear aperture. Thus, the gross material mass of the SOIE meniscus is 0.73 g and it is only 0.42 g for our Fresnel lens. The corresponding heat to drain off to decrease the temperature of our germanium Fresnel lens from 293 K (room temperature) to 90 K (operating temperature of industrial coolers) is equal to 23 J instead of 76 J for the SOIE silicon meniscus. The smaller the heat the shorter the cool down time.

Because a thickness of 500 μm is close to the thickness of standard cold filters, the Fresnel lens could even directly replace the cold filter of the DDCA. It should be noted that the Fresnel lens has a significant role to play in terms of the reduction of the edge sag of the integrated optics. Indeed, the 1.6 mm of the highest edge sag of the meniscus of the SOIE camera prevented from reaching an optical center thickness smaller than a few hundreds of micrometers.

D. Theoretical Performances

The first-order Fresnel lens is known to exhibit a strong chromaticity. However, as mentioned above, in this paper a high-order Fresnel lens has been selected because of its advantages in terms of chromatism. It is interesting to show here that our lens can effectively operate over the whole spectral range of interest, from 3 to 5 μm.

First, a high-order Fresnel lens operating in nominal order m_0 at nominal wavelength λ_0 is considered. In case of a Fresnel lens with the optical system aperture stop in the lens plane, the scalar diffraction efficiency at wavelength λ in order m is given by the following equation [27]:

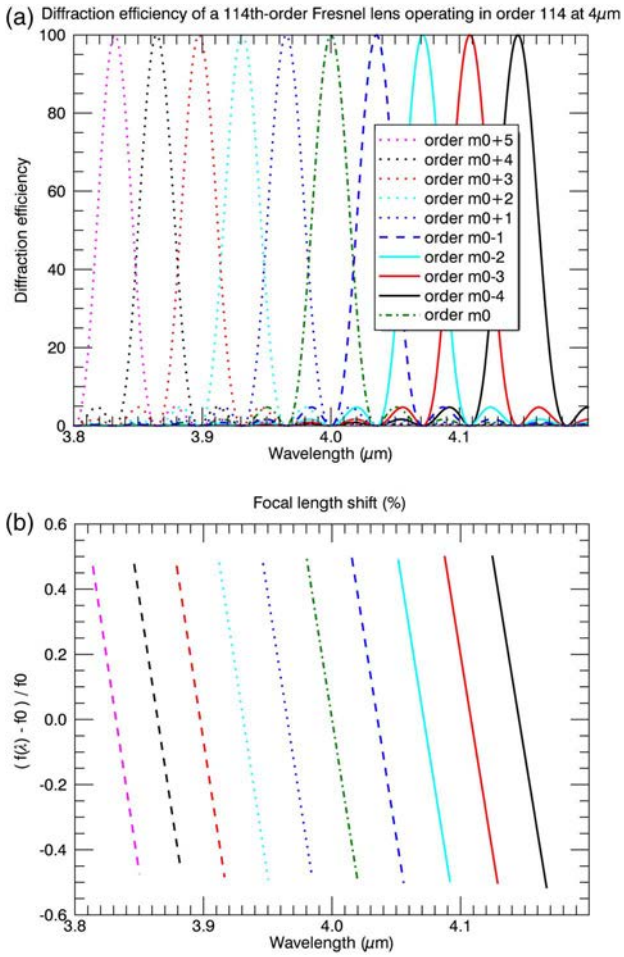

Fig. 4. (a) Illustration of the diffraction efficiency variation versus wavelength in the spectral bandwidth [3.8–4.2] μm for a high-order Fresnel lens operating in nominal order $m_0 = 114$ at nominal wavelength $\lambda_0 = 4$ μm. (b) Corresponding value of the defocus shift.

$$\eta_{m,\lambda} = \mathrm{sinc}^2\left(m - \frac{\lambda_0(n(\lambda) - 1)}{\lambda(n(\lambda_0) - 1)} m_0\right). \quad \textbf{(1)}$$

And the corresponding focal length at wavelength λ obeys:

$$f(\lambda) = \frac{m_0\lambda_0}{m\lambda} f_0, \quad \textbf{(2)}$$

where m is the most efficient diffraction order at wavelength λ and f_0 is the design focal length, i.e., $f_0 = f(\lambda_0)$.

In the paraxial approximation, a Fresnel lens with stop in contact that is etched in a germanium plate with a depth of 150 μm operates in nominal order $m_0 = 114$ at nominal wavelength $\lambda_0 = 4$ μm. In these conditions, the diffraction efficiency peaks at 100% at many wavelengths around the nominal wavelength [see Fig. 4(a)]. Moreover, according to Eq. (2), at all these wavelengths the focal length is equal to the design focal length f_0 and the Fresnel lens does not exhibit chromatism [see Fig. 4(b)]. Throughout the 3–5 μm spectral range, it exists around 50 wavelengths at which chromatic aberrations are equal to zero. The mean focal length shift from 3 to 5 μm is around ±0.5% which corresponds to around ±45 μm. This is less than the $\pm N t_{\mathrm{pix}} = \pm 60$ μm theoretical geometrical

depth of field estimated for a numerical aperture $N = 4$ and a pixel size $t_{pix} = 15$ μm. Thus, axial chromatic aberrations inherent in diffractive optics remain essentially negligible in the configuration of our Fresnel lens with the aperture stop in the lens plane.

In reality, the optical architecture of the proposed camera is a landscape lens configuration with aperture stop placed some distance away in front of the high-order Fresnel lens. As will be shown below from experimental results, this involves peculiar diffractive effects.

4. EXPERIMENTAL VALIDATION

A. Realization of the Camera

A prototype of our camera has been assembled and is illustrated in Fig. 5. On the left a view of inside of the laboratory dewar is presented: an optical housing which plays the role of the cold shield as well, holds the Fresnel lens in front of the detector. On the picture, we see the cold shield optically opened by the cold stop. The Fresnel lens and the detector array are hidden behind the cold stop.

On the picture, the object side of the setup may be seen with the position of the aperture stop shown by an arrow. The Fresnel lens and the detector array are hidden behind the aperture stop. On the figure on the right the overall system with Fresnel lens integrated inside the laboratory dewar is shown. Whereas the overall SOIE camera shown in Fig. 2(b) is a demonstrator integrated with a cryocooler, the system shown here in Fig. 5(b) is a laboratory prototype that works with a dewar manually filled with liquid nitrogen. The camera with the Fresnel lens would have the same size as the SOIE camera if used in a cryocooler.

Our 15 mm diameter germanium Fresnel lens whose size is compared to a coin is illustrated in Fig. 6. It has been diamond turned by Savimex company and it is made of 4 useful diffractive zones.

B. Characterization of the Camera

Several measurements have been made to evaluate the optical performances of our camera. Indeed, the polychromatic modulation transfer function (MTF) of our system as well as the noise equivalent temperature difference (NETD) have been estimated.

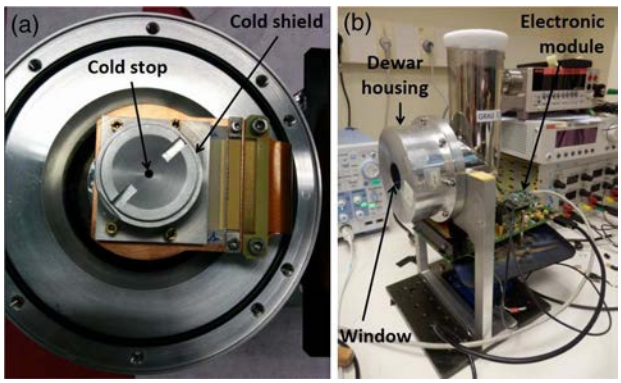

Fig. 5. (a) View of inside the laboratory dewar. (b) Picture of the overall camera.

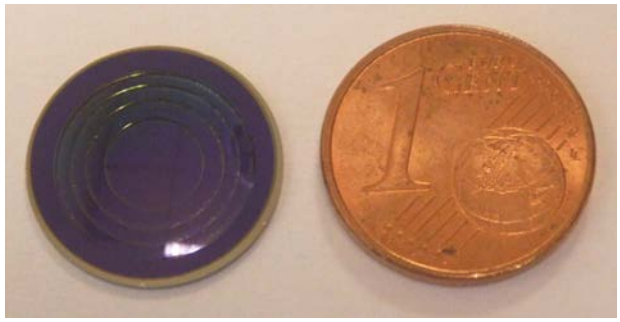

Fig. 6. Picture of the germanium Fresnel lens next to a one euro cent coin.

1. MTF Performance

As a first step, we aim at evaluating the optical performances of our camera over the field. Thus, the polychromatic MTF of our camera has been measured at different field angles using the *Spot Scan* method described in [16]. Our test bench is schematically drawn in Fig. 7. A blackbody illuminates a pinhole placed at the object focal plane of a collimator. The camera images that pinhole on the detector. We measure the signal delivered by the pixel whose intensity is maximum. It is our pixel of interest. Then we slightly move the camera in front of the collimator by subpixel shifts and for each position we measure the signal delivered by the pixel of interest. The displacement of the camera is made from rotational movements described by Euler angles. Thus, we obtain the well-sampled point spread function (PSF) of our imager. Then, the MTF is given by the absolute value of the Fourier transform of the PSF.

In Fig. 8 are shown the MTFs measured between 3.7 and 4.8 μm at six field angles from $\theta = 0°$ (on axis) to $\theta = 27°$ (edge of the length of the detector). The spatial frequency axis has a maximum value of 33 cycles/mm corresponding to the Nyquist frequency of our 15 μm pixel-pitch detector. The insets in Fig. 8 show the illuminated area of the Fresnel lens for each of the considered field angles.

In Fig. 8 our measurements are compared with theoretical MTF estimated by the Zemax optical design software from its infinitely thin Fresnel lens approximate model. Theoretical estimations are obtained after extraction of software data and taking into account the transfer function of the pixel. MTF curves show that experimental measurements stand below simple approximated data modeling. This could have been anticipated considering the fact that, like most others, this optical design software package does not accurately model the real shape of a

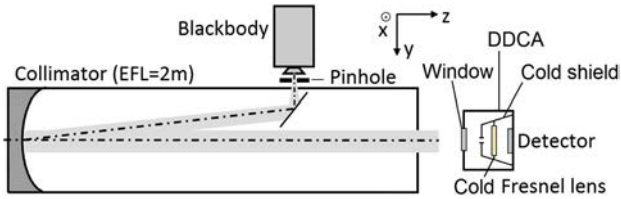

Fig. 7. Test bench for MTF measurements using the *Spot Scan* method.

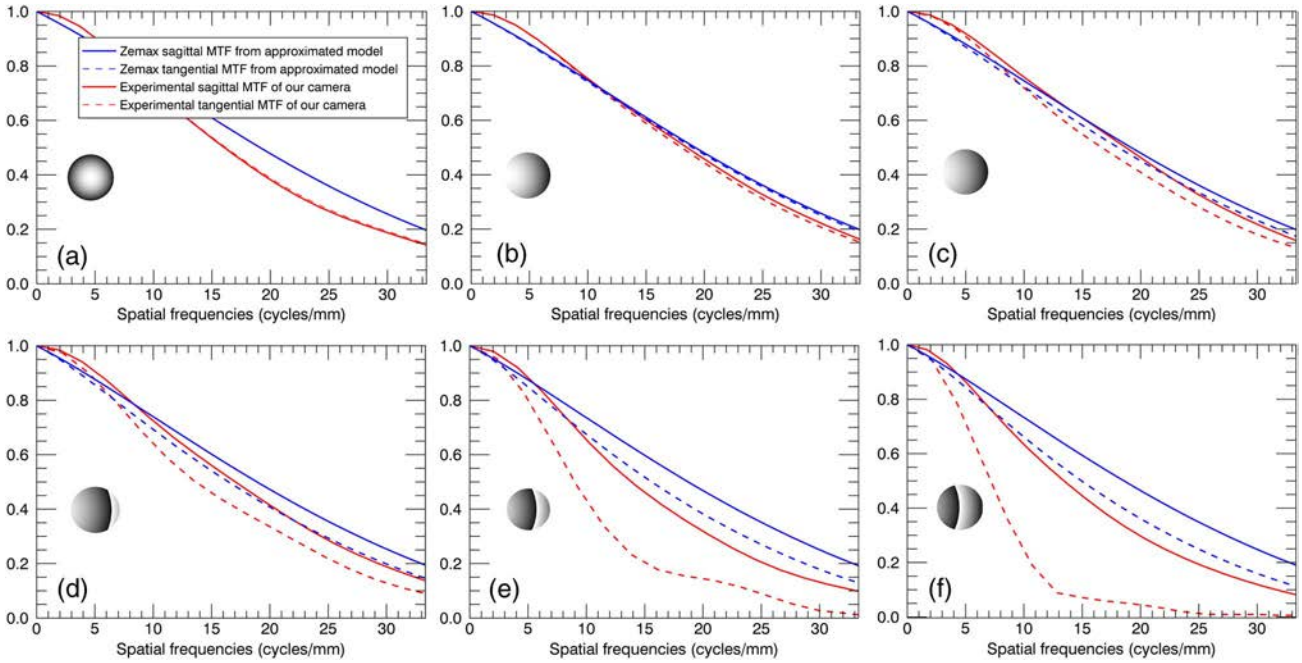

Fig. 8. System MTF of our camera from 3.7 to 4.8 μm for different field angles θ. (a) $\theta = 0°$, (b) $\theta = 10°$, (c) $\theta = 15°$, (d) $\theta = 20°$, (e) $\theta = 23°$, (f) $\theta = 27°$. The maximum abscissa value corresponds to the Nyquist frequency of the detector. The six insets show the illuminated area of the Fresnel lens for each field angle.

high-order Fresnel lens. Instead, it approximates it as an ideal infinitely thin component. Moreover, optical design software packages consider only one diffraction order. Thus, only standard chromatic aberrations are considered and diffractive chromatic aberrations are not properly taken into account. Consequently, optical design software generally model overly optimistic performances.

From Fig. 8 it can also be noted that as the field angle increases, the experimental MTF tends to drop in the radial direction, corresponding to the orientation direction of the Fresnel lens discontinuities. As shown by curves from software simulations, the field aberrations of our system remain limited. Thus the MTF degradation would not be due to geometrical out-of-axis aberrations but it rather seems to be directly linked to the diffractive optical element aberrations that are neglected by the optical design software.

Experimental MTF measured with our camera have also been compared with the experimental MTF measured with the SOIE camera. In Fig. 9 the comparison is done at three field angles corresponding to an on-axis measurement ($\theta = 0°$), a measurement at the edge of the width of the detector ($\theta = 23°$) and a measurement at the edge of the length of the detector ($\theta = 27°$). We notice that on-axis resolutions of the two cameras are similar but the off-axis performances of our camera at the edges of the detector are lower than the performances of the SOIE camera. The difference between the two prototypes lies essentially in the tangential direction.

A general design rule for photographic application demands a contrast standing above 0.3 at half-Nyquist frequency. Our camera fulfills this requirement up to around $\theta = 20°$ [see Fig. 8]. Thus, even though the performances of our camera are degraded at the edges of the detector, they remain fairly

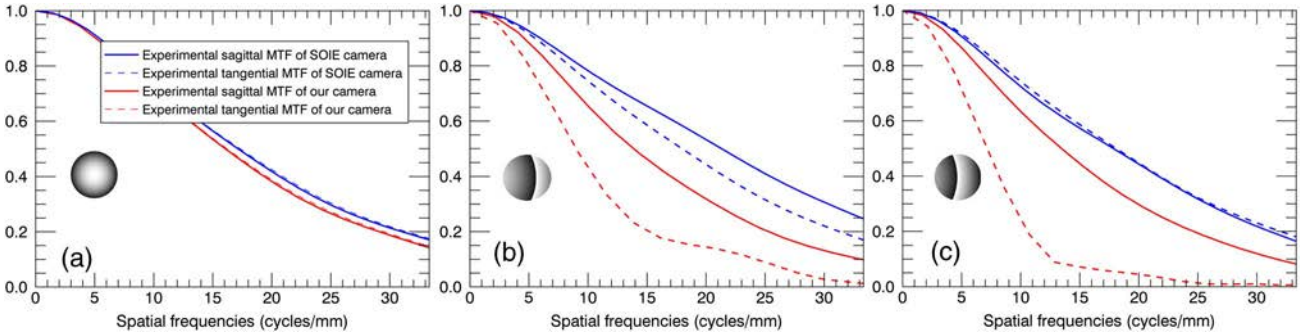

Fig. 9. Experimental MTF of our camera compared with the experimental MTF of SOIE camera. Results are given at different field angles θ. (a) $\theta = 0°$, (b) $\theta = 23°$, (c) $\theta = 27°$.

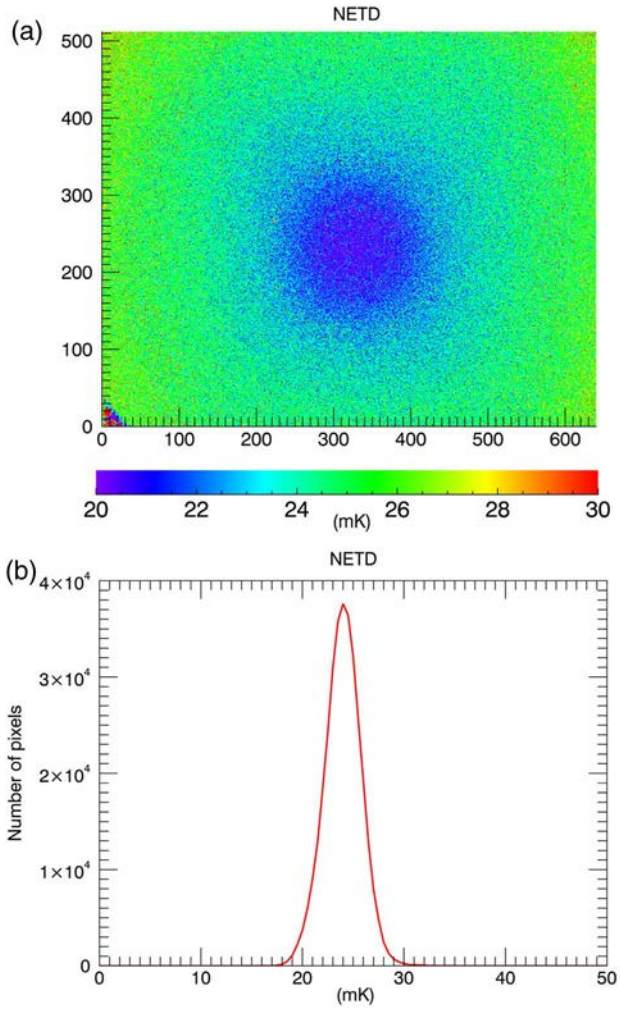

Fig. 10. (a) NETD 2D map (25°C, F/4, 50% well fill). (b) Corresponding NETD histogram.

acceptable on the most of the image field, as will be shown below indeed.

2. Noise Equivalent Temperature Difference

The NETD is defined as the temperature difference that would produce a signal-to-noise (SNR) equal to unity. It provides a measurement of the camera sensitivity. From a practical point of view, it is measured as the ratio of temperature difference between a hot temperature T_H and a reference temperature T_{Ref} to the corresponding signal-to-noise ratio. The SNR is itself defined as the ratio of the signal difference between two flat blackbody images Img_{T_H} and $\text{Img}_{T_{\text{Ref}}}$, respectively acquired at temperatures T_H and T_{Ref}, to the noise σ_{T_H} at temperature T_H [see Eq. (3)].

$$\text{NETD} = \frac{(T_H - T_{\text{Ref}})}{\text{SNR}} = \frac{(T_H - T_{\text{Ref}})}{\frac{\text{Img}_{T_H} - \text{Img}_{T_{\text{Ref}}}}{\sigma_{T_H}}} \quad (3)$$

$T_H = 25°\text{C}$ and $T_{\text{Ref}} = 20°\text{C}$ have been chosen here. The measured mean NETD at 50% well fill is around 24.22 mK ± 1.90 mK at 25°C and F/4. Figure 10(a) shows the NETD 2D map over the entire SCORPIO detector. In Fig. 10(b) is the corresponding histogram of the NETD. It is worth mentioning that a high quality NETD is achieved and that a similar NETD value was obtained with the SOIE camera in [4].

Fig. 11. Illustration of outdoor images taken from our camera.

Fig. 12. (a) Illustration of an indoor image taken from our camera and (b) compared to an image taken with the SOIE camera [4].

3. Experimental Images

Some images have been acquired with our prototype under different operating conditions. In Fig. 11 two outdoor images are shown after nonuniformity correction and bad pixels identification and replacement. On the left some people can be detected and recognized. On the right a landscape including buildings and vegetation is recorded.

Then the visual appearance of two images taken respectively with our camera and with the SOIE camera has been compared. An indoor picture from our prototype is shown in Fig. 12(a). It has been taken in a room. An image recorded in similar conditions with the SOIE camera is illustrated in Fig. 12(b). It is interesting to see that these two pictures have approximately the same quality.

Even though the edges of pictures recorded with our prototype are expected to be blurred in view of the measured MTF shown above (see Fig. 8), many details of the scene can be perceived in those images. Our camera can be seen as a real infrared eye with foveal vision: in the peripheral areas the image quality is degraded but the quality remains good in the center. We think that our prototype is compatible with various applications such as a aid-guidance for example.

5. CONCLUSION

A compact cooled infrared camera has been designed, manufactured and characterized. It works in the spectral band from 3 to 5 μm and is completely integrated inside the DDCA. The prototype is inspired from a former prototype called SOIE described in [4]; it has the same optical characteristics (horizontal

field of view of ±60°, F-number of 4, effective focal length of 9.6 mm) but the cold meniscus of the SOIE camera is replaced by a 500 μm-thick parallel plate made of germanium with a Fresnel profile etched on its detector-side surface. The use of a Fresnel lens has permitted to reduce the useful optical mass integrated inside the DDCA by a factor two. And above all the Fresnel lens is shown to have a relatively low impact on the image quality. Because the optics we propose has a thickness close to the thickness of standard cold filters, it could directly replace the cold filter of the DDCA. Thus, we would give an imaging property to the DDCA without any added optical mass in order to limit the cooling time process.

Funding. French Procurement Agency (DGA).

REFERENCES

1. M. Singer, "Design of a cryogenic IR detector with integrated optics," Proc. SPIE **7660**, 76601Z (2010).
2. R. C. Gibbons, S. H. Black, and R. N. Mullins, "System and method for viewing an area using an optical system positioned inside of a dewar," U. S. Patent 8,294,103 (23 October 2012).
3. G. Druart, N. Matallah, N. Guérineau, S. Magli, M. Chambon, P. Jenouvrier, E. Mallet, and Y. Reibel, "OSMOSIS: a new joint laboratory between SOFRADIR and ONERA for the development of advanced DDCA with integrated optics," Proc. SPIE **9070**, 90700Q (2014).
4. G. Druart, F. de la Barrière, N. Guérineau, J. Deschamps, M. Fendler, N. Lhermet, J. Rullière, S. Magli, Y. Reibel, and J. B. Moullec, "Towards infrared DDCA with an imaging function," Proc. SPIE **8012**, 801228 (2011).
5. F. de la Barrière, G. Druart, N. Guérineau, and J. Taboury, "Design strategies to simplify and miniaturize imaging systems," Appl. Opt. **50**, 943–951 (2011).
6. J. Tanida, T. Kumagai, K. Yamada, S. Miyatake, K. Ishida, T. Morimoto, N. Kondou, D. Miyazaki, and Y. Ichioka, "Thin observation module by bound optics (TOMBO): concept and experimental verification," Appl. Opt. **40**, 1806–1813 (2001).
7. F. de la Barrière, G. Druart, N. Guérineau, G. Lasfargues, M. Fendler, N. Lhermet, and J. Taboury, "Compact infrared cryogenic wafer-level camera: design and experimental validation," Appl. Opt. **51**, 1049–1060 (2012).
8. G. Druart, N. Guérineau, J. Taboury, S. Rommeluère, R. Haïdar, J. Primot, M. Fendler, and J.-C. Cigna, "Compact infrared pinhole fish-eye for wide field applications," Appl. Opt. **48**, 1104–1113 (2009).
9. A. Davis, R. C. Bush, J. C. Harvey, and M. F. Foley, "Fresnel lenses in rear projection display," in *Society for Information Display* (2001), Vol. **XXXII**, pp. 934–937.
10. M. G. Montes, J. C. Martinez-Anton, D. Vazquez Molini, A. A. Fernandez-Balbuena, and E. Bernabeu, "Achromatic Fresnel lens with improved efficiency for PV systems," Int. J. Photoenergy **2014**, 787392 (2014).
11. F. Languy and S. Habraken, "Nonimaging achromatic shaped Fresnel lenses for ultrahigh solar concentration," Opt. Lett. **38**, 1730 (2013).
12. G. Mikula, A. Kolodziejczyk, M. Makowski, and M. Sypek, "Optical diffractive elements for medical applications," Proc. SPIE **5954**, 59540Q (2005).
13. Y. Takizawa, A. Z. Marchi, R. Young, and Y. Takahashi, "JEM-EUSO optics design and its performance," *Proceedings of the 31st ICRC*, Lodz, Poland, 7–15 July 2009.
14. J. Bai, W. Hu, N. Guo, W. Lei, Y. Lv, X. Zhang, J. Si, X. Chen, and W. Lu, "Performance optimization of InSb infrared focal-plane arrays with diffractive microlenses," J. Electron. Mater. **43**, 2795–2801 (2014).
15. J. Suszek, A. M. Siemon, N. Blocki, M. Makowski, A. Czerwinski, J. Bomba, A. Kowalczyk, I. Ducin, K. Kakarenko, N. Palka, P. Zagrajek, M. Kowalski, E. Czerwinska, C. Jastrzebski, K. Switkowski, J.-L. Coutaz, A. Kolodziejczyk, and M. Sypek, "High order kinoforms as a broadband achromatic diffractive optics for terahertz beams," Opt. Express **22**, 3137 (2014).
16. T. Grulois, G. Druart, N. Guérineau, A. Crastes, H. Sauer, and P. Chavel, "Extra-thin infrared camera for low-cost surveillance applications," Opt. Lett. **39**, 3169 (2014).
17. D. Falkis and G. M. Morris, "Spectral properties of multiorder diffractive lenses," Appl. Opt. **34**, 14 (1995).
18. D. W. Sweeney and G. E. Sommargren, "Harmonic diffractive lenses," Appl. Opt. **34**, 2469 (1995).
19. Z. Liping, L. Y. Loy, Z. Yan, and Y. Zhisheng, "Achromatic design strategies with diffractive optical elements," Proc. SPIE **3897**, 624 (1999).
20. L. N. Hazra and C. A. Delisle, "Higher order kinoform lenses: diffraction efficiency and aberrational properties," Op. Eng. **36**, 1500–1507 (1997).
21. R. Gläbe and O. Riemer, "Diamond machining of micro-optical components and structures," Proc. SPIE **7**, 771602 (2010).
22. P. N. Blake and R. O. Scattergood, "Ductile regime machining of germanium and silicon," J. Am. Ceram. Soc. **73**, 949–957 (1990).
23. R. A. Clark, "Design specification of diamond turned optics," Proc. SPIE **38**, 164–183 (1991).
24. R. L. Rhorer and C. J. Evans, "Fabrication of optics by diamond turning," in *OSA Handbook of Optics*, 2nd ed, Vol. **1** (McGraw-Hill, 1995).
25. J. Yan, K. Maekawa, J. Tamaki, and T. Kuriyagawa, "Micro grooving on single-crystal germanium for infrared Fresnel lenses," J. Micromech. Microeng. **15**, 1925 (2005).
26. Y. Fan, Y. Zhu, and W. Pan, "Ultra-precision cutting of Fresnel lenses on single crystal germanium and the machining processing analysis," Proc. SPIE **7655**, 76550R (2010).
27. G. J. Swanson, "Binary optics technology: The theory and design of multi-level diffractive optical elements," Technical report 854 (Massachussetts Institute of Technology, Lincoln Laboratory, 1989).